Opto-Electronic Advances

ISSN 2096-4579 CN 51-1781/TN

Microsphere femtosecond laser sub-50 nm structuring in far field via non-linear absorption

Zhenyuan Lin, Kuan Liu, Tun Cao and Minghui Hong

Citation: Lin ZY, Liu K, Cao T, Hong MH. Microsphere femtosecond laser sub-50 nm structuring in far field via non-linear absorption. *Opto-Electron Adv* **6**, 230029(2023).

https://doi.org/10.29026/oea.2023.230029

Received: 20 February 2023; Accepted: 18 April 2023; Published online: 23 May 2023

Opto-Electronic Advances

Article

June 2023, Vol. 6, No. 6

DOI: 10.29026/oea.2023.230029

Microsphere femtosecond laser sub-50 nm structuring in far field via non-linear absorption

Zhenyuan Lin[1,3], Kuan Liu[2], Tun Cao[2*] and Minghui Hong[1,3*]

Creation of arbitrary features with high resolution is critically important in the fabrication of nano-optoelectronic devices. Here, sub-50 nm surface structuring is achieved directly on Sb_2S_3 thin films via microsphere femtosecond laser irradiation in far field. By varying laser fluence and scanning speed, nano-feature sizes can be flexibly tuned. Such small patterns are attributed to the co-effect of microsphere focusing, two-photons absorption, top threshold effect, and high-repetition-rate femtosecond laser-induced incubation effect. The minimum feature size can be reduced down to ~30 nm (λ/26) by manipulating film thickness. The fitting analysis between the ablation width and depth predicts that the feature size can be down to ~15 nm at the film thickness of ~10 nm. A nano-grating is fabricated, which demonstrates desirable beam diffraction performance. This nano-scale resolution would be highly attractive for next-generation laser nano-lithography in far field and in ambient air.

Keywords: non-linear effect; microsphere; femtosecond laser; far field

Lin ZY, Liu K, Cao T, Hong MH. Microsphere femtosecond laser sub-50 nm structuring in far field via non-linear absorption. *Opto-Electron Adv* **6**, 230029 (2023).

Introduction

In the past centuries, the creation of smaller features is of paramount importance in nanofabrication to explore unique opportunities to achieve new applications in material sciences[1], nano-photonics[2], and nano-biotechnology[3]. The development of nano-fabrication technology is driven by the need to increase the density of components and performance, which requires high accuracy in material processing and the capability of manufacturing in an atmospheric environment. Nevertheless, large area nano-creation toward higher resolution has proven to be increasingly challenging as feature sizes keep decreasing by using traditional methods, including extreme ultraviolet lithography[4], electron beam lithography[5], and reactive ion etching[6]. Compared to other advanced processing methods, laser precision engineering has been recognized as one of the most extensively used tools for micro/nano-structuring in the past centuries[7–11]. Owing to the feature of low heat affected zone (HAZ), ultrafast laser processing is well adapted to the high-quality micro-fabrication of soft materials, such as biological tissues[12] and hard or brittle materials[13]. The suppression of heat diffusion to the surroundings improves the spatial resolution of nano-creations. Non-linear absorption is another important benefit of ultrafast laser processing[14,15]. When processing transparent materials, such as glass and wide bandgap materials, with ultrafast laser pulses, the excitation of electrons from valence band (VB) to conduction band (CB) is initiated by non-linear absorptions, including multi-photon absorption or

[1]Pen-Tung Sah Institute of Micro-Nano Science and Technology, Xiamen University , Xiamen 361102, China; [2]School of Optoelectronic Engineering and Instrumentation Science, Dalian University of Technology, Dalian 116024, China; [3]Department of Electrical and Computer Engineering, National University of Singapore, 4 Engineering Drive 3, 117576, Singapore.

*Correspondence: MH Hong, E-mail: elehmh@xmu.edu.cn; T Cao, E-mail: caotun1806@dlut.edu.cn

Received: 20 February 2023; Accepted: 18 April 2023; Published online: 23 May 2023

tunnel ionization[16,17]. Using ultrafast lasers in materials processing can substantially reduce the fluctuation associated with optical breakdown threshold and improve reproducibility by tuning the laser processing parameters.

Complicated structures can be precisely made through ultrafast laser direct writing[18,19]. However, the key challenge of the ultrafast laser processing to produce extremely small features is the optical diffraction limit. To overcome such difficulty, various laser-based techniques have emerged for sub-diffraction processing, such as near-field scanning optical microscope patterning[20], interference lithography[21,22], and stimulated emission depletion microscopy[23], as well as multi-photons absorption lithography[24]. Sub-50 nm nanostructures have been also achieved by multiple femtosecond laser overlapping irradiation in far-field. However, the HAZ via these techniques is still much larger than the nano-structures, which mostly exhibit >300 nm melting zone[25,26]. Using a dielectric microsphere as a near-field lens for super-resolution nano-imaging and nano-fabrication has attracted great research interest[27,28]. The optical phenomenon known as photonic nano-jet can also contribute to laser beam focusing to overcome the diffraction limit. To increase the microsphere ultrafast laser processing throughput, the self-assembly method[29] and micro-lens arrays lithography[30] have been developed to fabricate surface patterns at a fast speed and low cost. In addition to nano-hole structures achieved by contact mode, the microsphere femtosecond laser fabrication can also realize arbitrary structures on sample surfaces in non-contact mode. By lifting the microsphere up to form a gap between sample and microsphere, the working distance (WD) can be increased to several micrometers. This strategy leads to the microsphere working in far field. In this case, the feature size of surface structures can only be reduced to ~300 nm by the 405 nm lamp[31], 512 nm, and 800 nm femtosecond laser irradiation[32,33], which is still far from the optical diffraction limit. Thus, how to achieve a good balance between the WD and feature size is a vital issue for the microsphere laser fabrication.

In this paper, the nano-structuring with feature size <50 nm is achieved on Sb_2S_3 thin films by non-contact microsphere femtosecond laser irradiation in far field and in ambient air. The surface nano-ablation is attributed to the extreme focus ability of the microsphere, the femtosecond laser high-repetition-rate incubation effect, and the non-linear effect associated with the femtosecond laser irradiation. The ablation depth and width of surface nano-structures are well tuned by laser fluence and scanning speed, while the achieved maximum depth and minimum width are ~40 nm and ~30 nm, respectively. The ablation results at different thicknesses, and the related linear fitting analyses predict that the feature size can be down ~15 nm at the film thickness of ~10 nm. Arbitrary surface nano-structures are realized, and the fabricated grating structures perform desirable optical properties, which reveals that this novel approach is a promising and feasible way to achieve surface nano-creation with excellent performance.

Materials and methods

The experimental setup of non-contact microsphere femtosecond laser irradiation is shown in Fig. 1(a). The femtosecond laser (Mira 900 of Coherent, Inc., 800 nm, 76 MHz) is focused by a microsphere via an objective lens (10×, 0.26 NA). The laser fluence is controlled by a half-wave plate and an isolator. The 470 nm light source is combined with the 800 nm femtosecond laser in the same optical path via two beamsplitters (BS), while the average ratios of reflectance and transmission are approximately 50∶50 at 470 nm and 40∶60 at 800 nm. The soda-lime glass microsphere of ~54 μm diameter (SLGMS, Cospheric) is fixed by a lens holder and aligned into a microscope system. The distance between the objective lens and the microsphere is equal to the focus length of the objective lens (~20 mm). The sample is put on a three-dimension (3D, XYZ) nano-stage with a minimum moving accuracy of 10 nm, a maximum speed of 5 mm/s, and a travel range of 20 mm (FS-3200P-WE2 series, OptoSigma). The nano-stage moving is automatically undertaken through an in-house programming code. The samples are amorphous Sb_2S_3 films at different thicknesses from 10 to 50 nm (prepared by magnetron sputtering deposition on silicon surfaces). Two charge-coupled devices (CCD) and a long WD objective lens are employed for the observation of focus position and working distance from top and side views. The related side view of the setup is shown in Fig. 1(b). It can be observed that the WD is ~8 μm, which means the focus length is ~35 μm (27 μm+8 μm). The focal length is about 44 times of the laser wavelength of λ=800 nm. Therefore, the microsphere femtosecond laser irradiation works in an optical far field. Near-field femtosecond laser fabrication mostly requires a smooth target surface due to its short working distance. Since the sub-50 nm ablation based on near-field effect is due to the

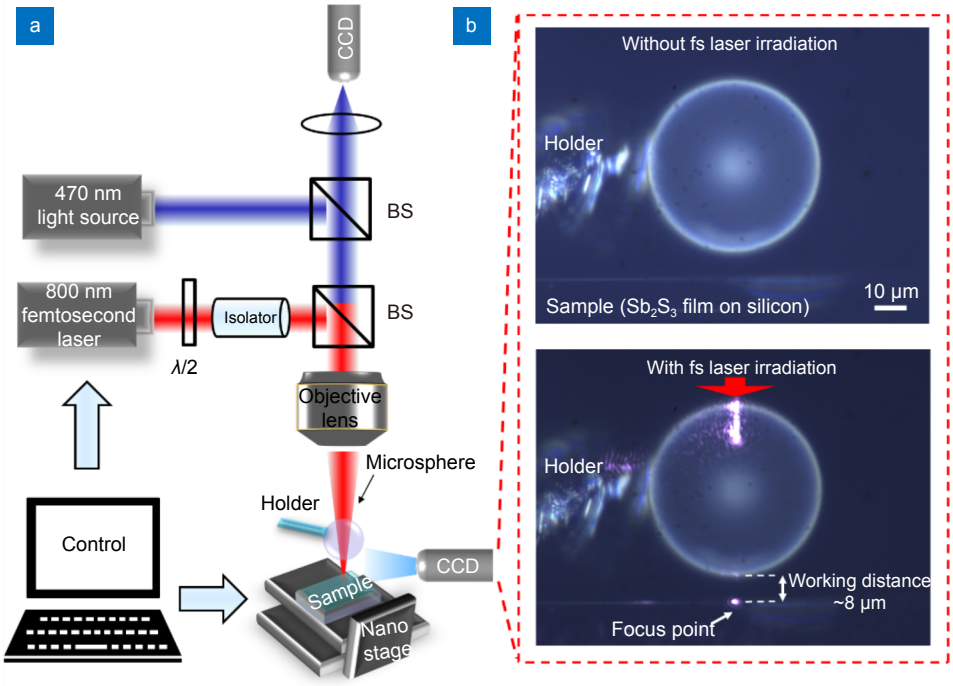

Fig. 1 | (**a**) Experimental setup of non-contact microsphere femtosecond laser irradiation. (**b**) Side view of microsphere focusing with femtosecond laser beam.

generation of evanescent waves, the ablated depths are shallow and mostly <10 nm[20,34]. For the microsphere femtosecond laser irradiation working in far field, the length of photonic nanojet is normally over several micrometers[32,35]. Thus, it is feasible to achieve a considerable ablation depth. By lifting the microsphere up, arbitrary surface patterning can be realized via the programming movement of the nano-stage.

Results and discussion

Surface nano-structuring in far field

The surface nano-creation is fabricated by the microsphere femtosecond laser irradiation in far field, as shown in Fig. 2(a), ~43 nm (λ/18) wide nano-lines with ~150 nm (λ/5) period are directly created on 30 nm thick Sb_2S_3 films at the laser fluence of 0.38 mJ/cm^2 and the scanning speed of 100 μm/s. The nano-lines have a sharp boundary and smooth edge. For the previously reported microsphere laser working in near field, the melting zone is obvious after laser irradiation[31,36]. In our experiments, the localized heating of the Sb_2S_3 thin films via the microsphere focusing drastically increases the temperature on the irradiated area. There is no apparent surface melting or damage on the ablated edge of the Sb_2S_3 film surface, which means the thermal diffusion to the surrounding around the femtosecond laser irradiation area is very small. Thus, the femtosecond laser irradiation via microsphere can create sub-50 nm nano-structures with high quality on the Sb_2S_3 thin films. The AFM image as well as the cross-sectional profile in Fig. 2(b, c) confirm that the ablation depth is ~30 nm, which indicates the Sb_2S_3 film is completely removed for the nano-lines with a depth-to-width ratio of 3∶4. It illustrates the capability far-beyond the diffraction limit fabrication by the microsphere femtosecond laser irradiation. Nano-structures with this feature size can be applied to fabricate different opto-electronics devices. Especially for the Sb_2S_3 thin films, which can exhibit tunable large bandgap (1.72~2.05 eV) and optical properties in the visible wavelength via the phase change[37], the high refractive index and low phonon frequency make Sb_2S_3 thin film attractive for applications that require high transmission from the visible to the mid-infrared region. The surface nano-creations on phase change materials are mostly realized via traditional methods, such as focused ion beam or electron beam lithographies[38,39]. Nevertheless, the low efficiency and high system cost inhibit large-area processing by these methods. Therefore, the microsphere femtosecond laser irradiation, which can realize sub-50 nm surface nano-creation in far field and in ambient air with high efficiency, is a feasible way to realize Sb_2S_3-based visible opto-electronics devices.

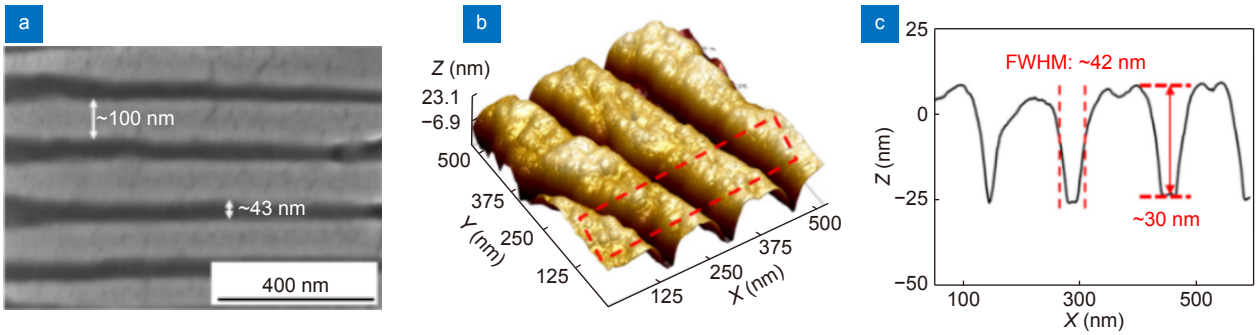

Fig. 2 | (**a**) SEM and (**b**) AFM images, as well as (**c**) corresponding cross-sectional profile of sub-50 nm nano-lines created at the laser fluence of 0.38 mJ/cm^2 and scanning speed of 100 μm/s.

Formation mechanism of sub-50 nm structures

The formation of such nano-structures relies on the co-effect of the microsphere focusing, high-repetition-rate femtosecond laser induced incubation effect, and the non-linear absorption of femtosecond laser irradiation. According to the experimental results and the physics behind laser interaction with materials, the formation mechanism of such nano-features can be divided into three processes, as illustrated in Fig. 3.

1) The first process is the small focusing capability of microsphere. The focusing behavior of microsphere can be calculated by finite-different time-domain (FDTD) method. Since the lime soda glass microsphere in our experiments have a size deviation of 10%, the diameter of the microsphere for the numerical calculation is set as 50 μm. As shown in Fig. 3(a), a plane wave (800 nm, *x*-polarized) propagates (along *z* axis) through a 50 μm lime soda glass microsphere (n_g=1.5172 at 800 nm). The microsphere diameter is much larger than the incident laser wavelength of 800 nm. The calculated focus length is ~31.4 μm with a ~4 μm depth of focus (radius: 25 μm, WD: 6.4 μm, see details in Fig. S1, Supplementary information), which is consistent with the measured WD shown in Fig. 1(b). The electric field intensity squared $|\boldsymbol{E}|^2$ distribution along *z* axis shows that the energy of the light field increases rapidly and is the highest at a distance of 6.4 μm from the exit facet of microsphere, where the $|\boldsymbol{E}|^2$ is approximately 1500 times of the incident electric field intensity squared ($|\boldsymbol{E}_0|^2 = 1$), as shown in Fig. S1(b). As described above, the required laser fluence for creating sub-50 nm nano-lines is only 0.38 mJ/cm^2 at the high repetition rate of 76 MHz. The intensity enhancement by the microsphere leads to the surface ablation. Then the intensity decreases rapidly with the distance in *z* direction and the length of the photonic nanojet is ~5 μm. This photonic nanojet is long enough to achieve the dozens of nanometers of ablation depth on the Sb_2S_3 thin films. The intensity profile of $|\boldsymbol{E}_x|^2$ (*x*-polarized) and $|\boldsymbol{E}_z|^2$ (*z*-polarized) along *x* axis at the maximum intensity position (*z*=6.4 μm) is plotted in Fig. S1(c), at which the calculated FWHM of the photonic nanojet is ~678 nm. This FWHM of intensity profile is much larger than the ablated feature size in Fig. 2. Thus, the microsphere focusing is not the only reason to create the sub-50 nm structures. However, the enhancement of electric field intensity via microsphere can localize the laser energy within a narrow area to achieve a high laser fluence at the focus position, which is an important factor for the subsequent non-linear effect. Meanwhile, considering the tight focusing condition, the distribution of $\boldsymbol{E}_z$ component surrounds the focus point, which leads to less debris and suppresses the laser-induced periodic surface structures (LIPSS) effect[40,41].

2) The second process is the two photons absorption (TPA) of the Sb_2S_3 films under the femtosecond laser irradiation. When the photon energy of incident beam is larger than the bandgap of irradiated material, an electron can be excited from VB to CB by the single-photon absorption. In the case of photon energy lower than the bandgap of the irradiated target, the excitation of an electron to a high energy state may require the absorption of two or more photons, which leads to the TPA or multi-photons absorption[42,43]. In our experiment, the photon energy of the 800 nm femtosecond laser (1.55 eV) is smaller than the bandgap of amorphous Sb_2S_3 thin film (2.05 eV)[37]. It requires at least two photons absorption for the excitation of an electron from VB to CB, as shown in Fig. 3(b). Due to the quadratic dependence of TPA on the laser fluence, the effective intensity profile becomes narrower by the absorption of two photons[44,45]. Through numerical calculation, the FWHM of the effective focal spot size for TPA is further reduced to ~500 nm.

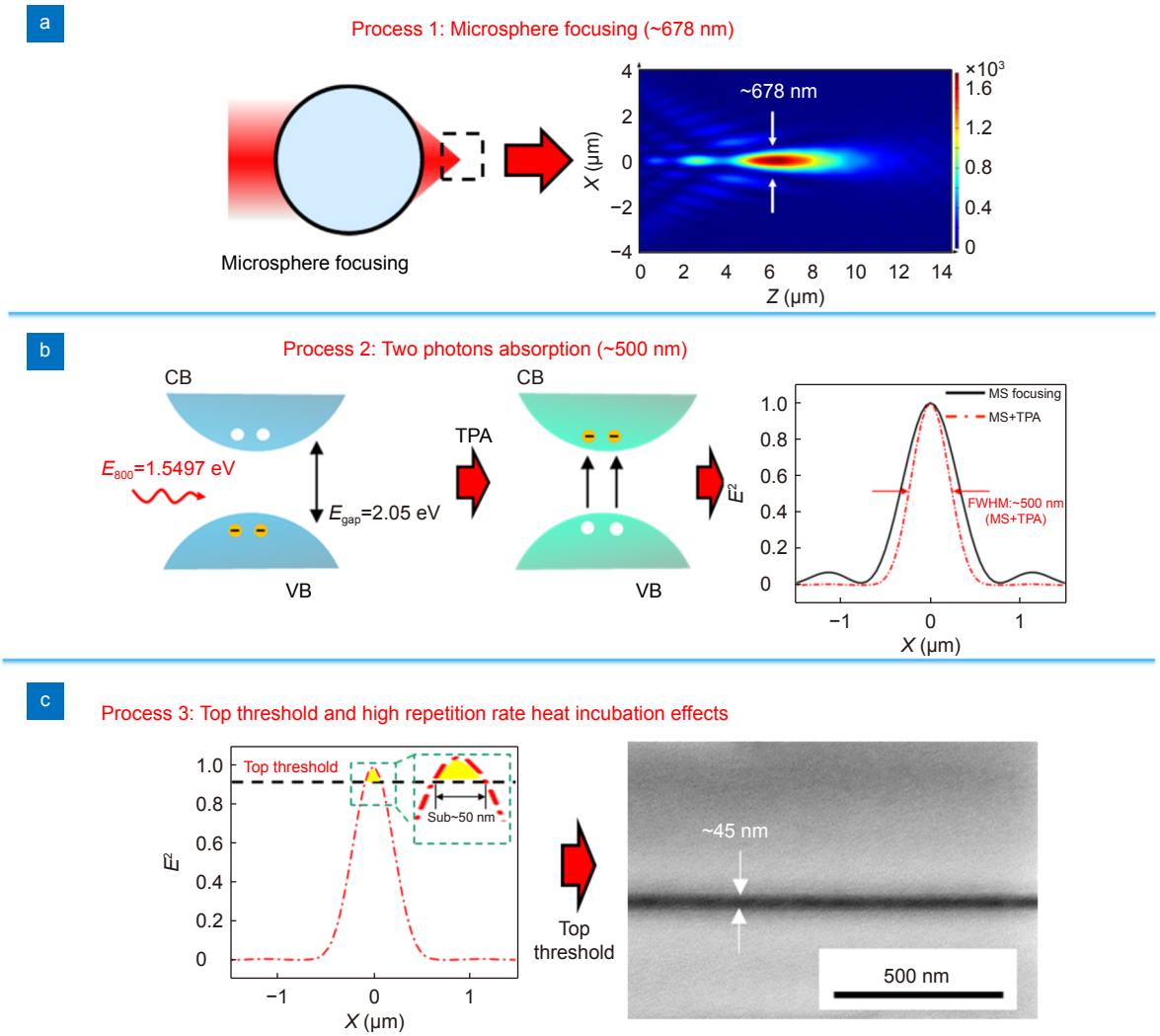

Fig. 3 | Formation mechanism of microsphere femtosecond laser irradiation. (**a**) Focusing via 50 μm microsphere by 800 nm laser irradiation. (**b**) TPA of Sb_2S_3 thin films under 800 nm femtosecond laser irradiation. (**c**) top threshold and high-repetition-rate femtosecond laser induced incubation effects.

Although it is still ~10 times of the FWHM of the ablation area achieved in our experiments, the narrow effective intensity profile due to the TPA also brings about the top threshold ablation effect, which can further reduce the ablation feature size.

3) The third process is the co-effect of the top threshold and high-repetition-rate heat incubation of the femtosecond laser irradiation. Because of the threshold effect of TPA, the laser fluence could be precisely controlled so that only a small portion of the focus spot exceeds the ablation threshold of target materials, resulting in feature size beyond the optical diffraction limit[46]. The threshold effect performs a highly non-linear dependence on femtosecond laser fluence, especially when the laser fluence is approaching the threshold. Since the resolution can always be improved if one keeps reducing the difference between the laser fluence and threshold value, in principle, there is no limit to the fabrication resolution when taking advantage of the threshold effect. So far, there is no theoretical description to define the exact feature size of surface nano-ablation, which results from the threshold effect. The reported studies have described that the feature size is mostly reduced to two-fifths of the original beam width due to the TPA[16]. By controlling the laser fluence and material properties, the effective feature size due to the top threshold can be <10% of the focusing beam width of the TPA absorption[47,48]. In our experiments, as shown in Fig. 3(c), through precisely tuning laser fluence and scanning speed, the top threshold effect of femtosecond laser irradiation keeps reducing the effective ablation area, and the ~45 nm line is achieved, which is only 9% of the calculated beam profile of the

TPA absorption. Considering the sub-50 nm ablation is realized under the high-repetition-rate femtosecond laser irradiation, the multi-pulses incubation effect should be another critical factor for the surface nano-creation. At the laser fluence of 0.38 mJ/cm^2 and the repetition rate of 76 MHz, the single pulse energy is only ~0.3 nJ. It is not high enough for the surface ablation of Sb_2S_3 thin films by single-pulse irradiation at such low pulse energy. At the repetition rate of 76 MHz, the interval between two individual laser pulses is ~12 ns. The femtosecond laser can increase the electron temperature rapidly due to its short duration, and then transfer the energy from electrons to lattices for the heating of lattices within several picoseconds. However, for the temperature decrease of lattice, the required time is normally on a scale of ~100 ns[49]. For the high-repetition-rate femtosecond laser irradiation, the heat accumulation is considerable at the multi-pulse irradiation with a short interval (12 ns) between pulses. The reported study has demonstrated that the absorption of Sb_2S_3 thin film at 800 nm is dependent on the temperature, while the absorption changes from <1% to >10% while the temperature increases from 200 to 250 °C[50]. During the high-repetition-rate femtosecond laser irradiation, the absorption of Sb_2S_3 thin film keeps increasing with temperature. This non-linear absorption change can lead to the incubation effect. Therefore, the sub-50 nm surface nano-structures on the Sb_2S_3 thin films are attributed to the co-effect of the microsphere focusing, non-linear absorption, and the high-repetition-rate incubation effect associated with the femtosecond laser irradiation.

Functional nano-structure fabrication and applications

To demonstrate the capability of arbitrary fabrication, more surface nano-structures are fabricated, as shown in Fig. 4. Nano-dot structures are created on ~30 nm thick Sb_2S_3 thin films at 7.6 ×10^5 pulse number (exposure time: 1 ms) and different laser fluences, as shown in Fig. 4(a–c). By changing laser fluence from 0.26 to 0.46 mJ/cm^2, the feature size of the nano-dots can be tuned from 35 to 80 nm (λ/26~λ/10) as well as ablation depth increases from 17 nm to 30 nm (see details AFM cross-section profiles in Fig. S2, Supplementary information). The flat bottoms shown in Fig. 4(b, c) indicate the 30 nm Sb_2S_3 thin films are removed completely at the laser fluence >0.42 mJ/cm^2. These nano-dots fabricated at different laser fluences reveal strong dependence between the ablation feature size and laser fluence. Depending on the laser parameters, nano-lines can be fabricated by tuning the scanning speed and laser fluence. At the scanning speed of 100 μm/s and laser fluence of 0.38 mJ/cm^2, the Sb_2S_3 thin film is ablated obviously, and a ~39 nm nano-line is created, as shown in Fig. 4(d). The edge of the ablated area is sharp, and no obvious damage is observed. In this case, the laser fluence is slightly higher than the threshold. Thus, the top threshold effect leads to the ablation of a feature size much smaller than the optical diffraction limit. Furthermore, as shown in Fig. 4(e), the width of the nano-line is increased to ~52 nm at a laser fluence of 0.42 mJ/cm^2, as well as the HAZ at the edge becomes obvious and the width of HAZ is ~30 nm. In Fig. 4(f), the width of nano-line and HAZ keep enlarging while the laser fluence increases to 0.46 mJ/cm^2. The melting becomes obvious around the ablated nano-line. It is attributed to the heat accumulation caused by the multi-pulse irradiation. The corresponding AFM image and cross-sectional profile shown in Fig. S3(a, b) show that the ablation depth is 30 nm, as well as the FWHM is ~80 nm, respectively. The formation and evolution of nano-lines are similar to the nano-dots in Fig. 4(a–c), which indicates the surface nano-structures of the Sb_2S_3 thin films can be well tuned by changing the scanning speed and laser fluence. More ablation results of nano-dots and nano-lines fabricated at different laser parameters are shown in Fig. S4. These nano-structures also show the non-linear and the incubation effects of the high-repetition-rate femtosecond laser irradiation play key roles in the surface nano-creation.

The microsphere femtosecond laser irradiation allows the free writing of arbitrary planar patterns with a controllable length, separation, and trajectory. In Fig. 4(g), triple nano-lines are fabricated at the linewidth of ~30 nm, and the spaces are from 100 to 300 nm. The creation of these nano-lines indicates the microsphere femtosecond laser irradiation is able to realize desirable nano-structures and make high-performance optical devices. As shown in Fig. 4(h), a wavy line of sub-100 nm width is fabricated at a laser fluence of 0.6 mJ/cm^2 and a scanning speed of 100 μm/s. The corresponding AFM image of the wavy nano-line is characterized in Fig. S3(c, d), while the ablation depth and the FWHM are ~30 nm and ~88 nm, respectively. There is no crack or damage on the corner of the curve. Double sub-50 nm wavy lines are also made at a laser fluence of 0.38 mJ/cm^2, as shown in Fig. 4(i). The minimum space between two

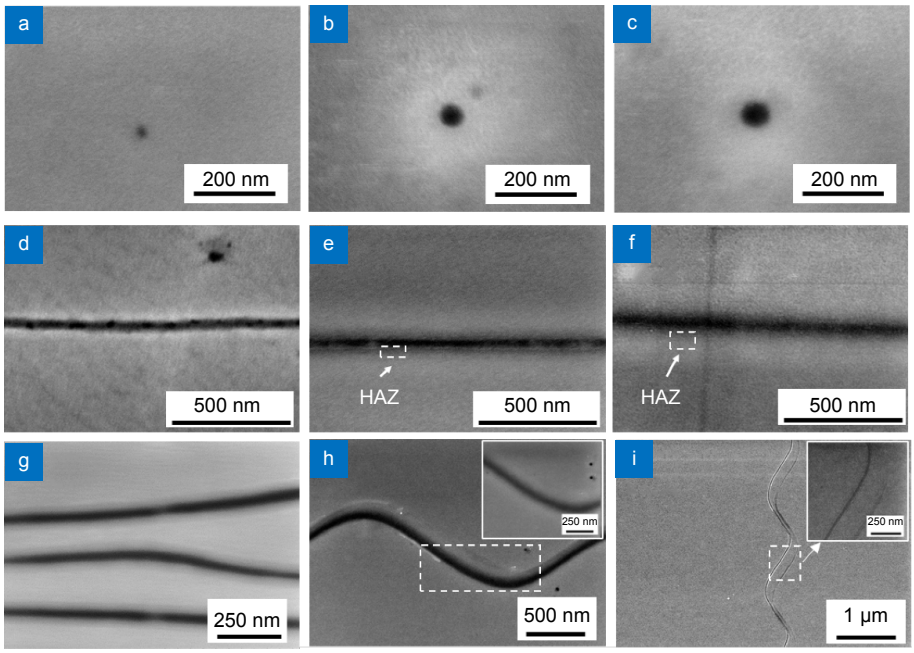

Fig. 4 | Different nano-structures created by microsphere femtosecond laser irradiation on 30 nm thick Sb_2S_3 thin films. Nano-dots fabricated at different laser fluences of (**a**) 0.30, (**b**) 0.42, and (**c**) 0.46 mJ/cm^2. Single nano-lines made at a scanning speed of 100 μm/s and different laser fluences of (**d**) 0.38, (**e**) 0.42, and (**f**) 0.46 mJ/cm^2. Irradiation results of arbitrary structures. (**g**) Irregular sub-50 nm triple nano-lines, (**h**) single sub-100 nm, and (**i**) double sub-50 nm wavy nano-lines.

nano-curves can be reduced to ~50 nm (λ/16). The successful creation of these complex nano-structures indicates that the microsphere femtosecond laser irradiation is suitable for the construction of arbitrary nano-patternings with high resolution and smoothness, which can be used for the nano-fabrication of opto-electronics devices. The relationship between the minimum FWHM and the depth is evaluated via surface nano-creation at different thick Sb_2S_3 thin films (25, 35, and 42 nm), as shown in Fig. 5. All these nano-structures are fabricated at a scanning speed of 100 μm/s. By the microsphere femtosecond laser irradiation, the minimum FWHM changes from 30 to 50 nm with the increase of thickness from 25 to 42 nm, as shown in Fig. 5(a–i). Depending on the ablation results at different thicknesses, the fitting analyses of the curve between the ablation depth and FWHM is plotted in Fig. 5(j). The distribution of the experimental results is approximately linear, and the FWHM increases with ablation depth, as well as the ratio of ablation depth and FWHM is ~0.7. According to the linear fitting analyses, the minimum ablation width can be evaluated at different thicknesses. As shown in Fig. 5(j), by extending the fitting line to the smaller or larger ablation depth (the dashed area), the corresponding FWHM can be tuned widely. At the ablation depth of 10 nm, the minimum FWHM can be reduced to ~15 nm (~λ/53).

The applications of surface nano-structures created by the microsphere femtosecond laser irradiation are demonstrated via the fabrication of diffractive gratings. Reflective gratings at a period of 1, 2, and 4 μm are designed and fabricated. The size of each diffractive grating structure is 1×1 mm^2. Uniform reflective grating structures of Sb_2S_3 thin films are fabricated on silicon surfaces. For a high diffraction efficiency of the grating at 532 nm incident light, the feature size of each unit is ~500 nm. The uniformity of the reflective gratings can be found in Fig. 6(a, c, e). The fabricated nano-structures are smooth. All the experimental and calculated values of diffraction angles at different grating structures are listed in Supplementary Table S1. The diffraction angles can be theoretically estimated by Eq. (1):

$$m\lambda = \Lambda\left(\sin\theta_m + \sin\theta_i\right) , \quad (1)$$

where m refers to the diffraction order, λ the wavelength of incident light, Λ the period width of the grating, θ_i the incident angle and θ_m the diffraction angle at different orders. The 532 nm laser at an incident angle of θ_i=15° irradiates on the grating structures and the charge coupled device captures the reflection laser spots. The diffraction results of the grating at a period of 1, 2, and 4 μm are shown in Fig. 6(b, d, g), respectively. In response to the 532 nm laser illumination, the grating at a period of 1 μm results in the first order at 15.8° (m=1) and

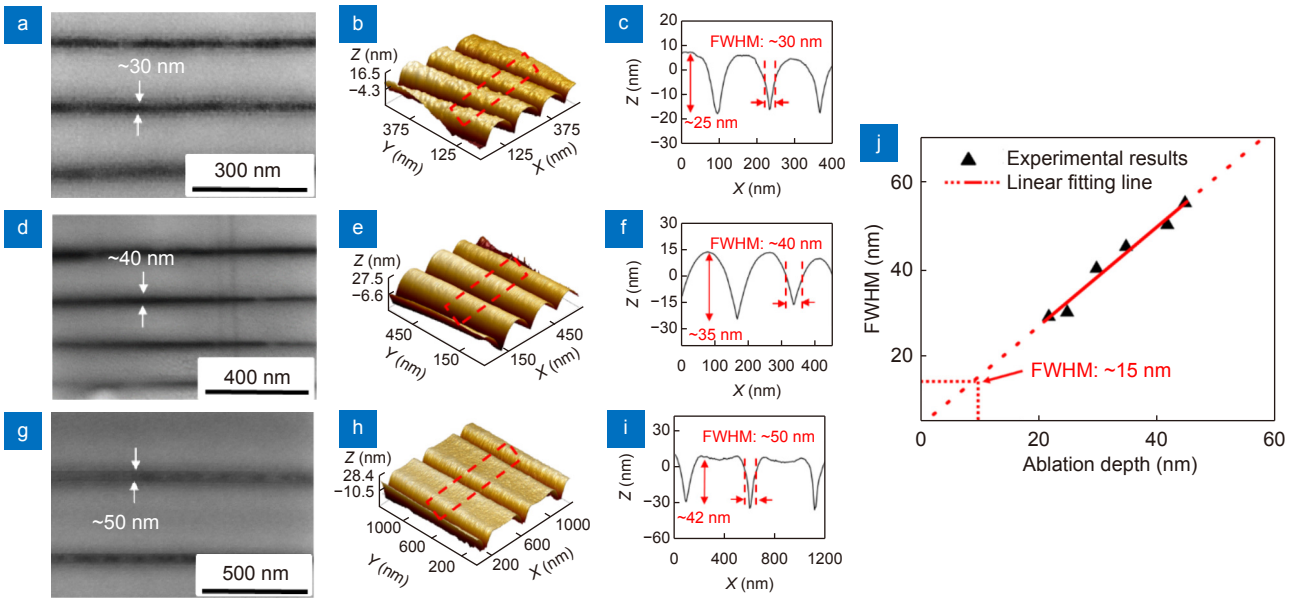

Fig. 5 | SEM and AFM images of the nano-structures created on Sb_2S_3 thin films at the film thickness of (**a**–**c**) ~25, (**d**–**f**) ~35, and (**g**–**i**) ~42 nm. (**j**) Linear fitting analysis of the FWHM vs ablation depth.

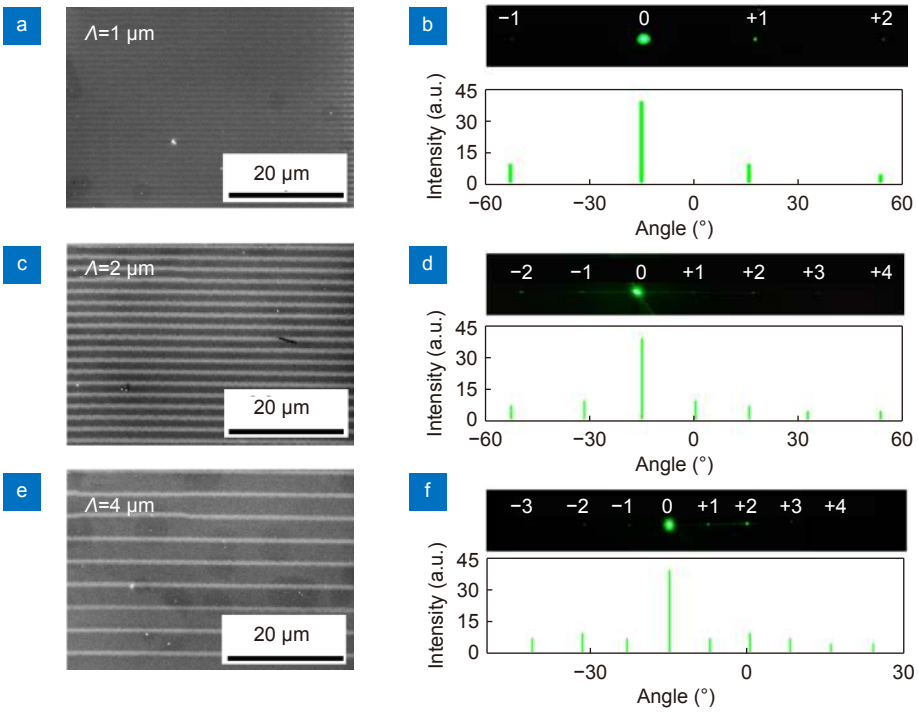

Fig. 6 | SEM images of the reflective grating by microsphere femtosecond laser irradiation at a period of (**a**) 1, (**c**) 2, and (**e**) 4 μm, respectively. The diffraction pattern, diffraction intensity, and angle observed in reflection for grating structures at a period of (**b**) 1, (**d**) 2, and (**f**) 4 μm, respectively. The number refers to the diffraction order of each reflective grating.

−52.6° (m=−1), which agrees well with the theoretical value of 16.1° (m=1) and −53.2° (m=−1). As the period of the grating changes to 2 μm, the laser diffraction beam spots increase with the first, second, third, and fourth orders (m>0) at 0.4°, 15.8°, 32.6°, and 53.61°, respectively. As for the period of 4 μm, the diffracted laser beam spots up to the 4th order with the diffraction angles from −7.2° to 32.6°, while the 5th order diffraction spot intensity is too weak to be recognized. When the period decreases, the number of the supported orders also reduces, and each supported order covers a larger diffraction angle. The deviation of the diffractive angel between the experimental results and theoretical calculation is less than 1°. The slight deviation between the experimental and

simulation results is attributed to the fabrication quality of the gratings. Further reducing the feature size to sub-50 nm makes it possible to fabricate more functional opto-electronics devices, especially for the realization of tunable visible metasurfaces. This strategy can be further improved. First of all, the optimal combination between the focus spot and working distance should be further tuned. The focus spot of microspheres can be reduced by using smaller microspheres[31,32,35]. However, the smaller microsphere means a shorter working distance. Thus, a balance between the focus spot size and working distance should be considered. The microsphere can also work in different conditions to increase the effective numerical aperture for a smaller focus spot. Furthermore, the optical property of microspheres can be adjusted by the engineered microsphere. Different focusing characteristics based on the engineered microspheres are reported, including spatial modulation[51] and multi-focusing[52], which can be used for the arbitrary surface nano-patterning directly. Therefore, the microsphere femtosecond laser irradiation has a great potential for the nano-fabrication of functional devices.

Conclusions

In this study, sub-50 nm nano-structures are successfully fabricated on Sb_2S_3 thin films via the microsphere femtosecond laser irradiation in far field and in ambient air. The feature size can be tuned flexibly by laser fluence, scanning speed, and thin film thickness. The fitting results based on the ablation width at different thicknesses predict that the feature size can be reduced down to ~15 nm at the film thickness of ~10 nm. The arbitrary surface structuring indicates the flexible patterning capability of the microsphere femtosecond laser irradiation. The fabrication and the excellent performance of surface grating structures show the large area processing ability and high uniformity of this strategy, which is significant for the nano-fabrication of functional devices.

References

1. Cummins C, Lundy R, Walsh JJ, Ponsinet V, Fleury G et al. Enabling future nanomanufacturing through block copolymer self-assembly: a review. *Nano Today* **35**, 100936 (2020).
2. Xiong YF, Xu F. Multifunctional integration on optical fiber tips: challenges and opportunities. *Adv Photonics* **2**, 064001 (2020).
3. Grebenko AK, Motovilov KA, Bubis AV, Nasibulin AG. Gentle patterning approaches toward compatibility with bio-organic materials and their environmental aspects. *Small* **18**, 2200476 (2022).
4. Wang L, Kirk E, Wäckerlin C, Schneider CW, Hojeij M et al. Nearly amorphous Mo-N gratings for ultimate resolution in extreme ultraviolet interference lithography. *Nanotechnology* **25**, 235305 (2014).
5. Ray D, Wang HC, Kim J, Santschi C, Martin OJF. A low-temperature annealing method for alloy nanostructures and metasurfaces: unlocking a novel degree of freedom. *Adv Mater* **34**, 2108225 (2022).
6. Karakachian H, Rosenzweig P, Nguyen TTN, Matta B, Zakharov AA et al. Periodic nanoarray of graphene pn-junctions on silicon carbide obtained by hydrogen intercalation. *Adv Funct Mater* **32**, 2109839 (2022).
7. Wolf A, Dostovalov A, Bronnikov K, Skvortsov M, Wabnitz S et al. Advances in femtosecond laser direct writing of fiber Bragg gratings in multicore fibers: technology, sensor and laser applications. *Opto-Electron Adv* **5**, 210055 (2022).
8. Ma ZC, Zhang YL, Han B, Chen QD, Sun HB. Femtosecond-laser direct writing of metallic micro/nanostructures: from fabrication strategies to future applications. *Small Methods* **2**, 1700413 (2018).
9. Qin L, Huang YQ, Xia F, Wang L, Ning JQ et al. 5 nm nanogap electrodes and arrays by super-resolution laser lithography. *Nano Lett* **20**, 4916–4923 (2020).
10. Lin ZY, Ji LF, Hong MH. Approximately 30 nm nanogroove formation on single crystalline silicon surface under pulsed nanosecond laser irradiation. *Nano Lett* **22**, 7005–7010 (2022).
11. Zhang JQ, Gao Y, Li C, Ju K, Tan JP et al. Laser direct writing of flexible antenna sensor for strain and humidity sensing. *Opto-Electron Eng* **49**, 210316 (2022).
12. Ma ZC, Zhang YL, Han B, Hu XY, Li CH et al. Femtosecond laser programmed artificial musculoskeletal systems. *Nat Commun* **11**, 4536 (2020).
13. Livakas N, Skoulas E, Stratakis E. Omnidirectional iridescence via cylindrically-polarized femtosecond laser processing. *Opto-Electron Adv* **3**, 190035 (2020).
14. Zhang YL, Tian Y, Wang H, Ma ZC, Han DD et al. Dual-3D femtosecond laser nanofabrication enables dynamic actuation. *ACS Nano* **13**, 4041–4048 (2019).
15. Saha SK, Wang DE, Nguyen VH, Chang YN, Oakdale JS et al. Scalable submicrometer additive manufacturing. *Science* **366**, 105–109 (2019).
16. Sugioka K, Cheng Y. Ultrafast lasers-reliable tools for advanced materials processing. *Light Sci Appl* **3**, e149 (2014).
17. Lin ZY, Hong MH. Femtosecond laser precision engineering: from micron, submicron, to nanoscale. *Ultrafast Sci* **2021**, 9783514 (2021).
18. Wang HT, Hao CL, Lin H, Wang YT, Lan T et al. Generation of super-resolved optical needle and multifocal array using graphene oxide metalenses. *Opto-Electron Adv* **4**, 200031 (2021).
19. Zhou WP, Bai S, Xie ZW, Liu MW, Hu AM. Research progress of laser direct writing fabrication of metal and carbon micro/nano structures and devices. *Opto-Electron Eng* **49**, 210330 (2022).
20. Lin Y, Hong MH, Wang WJ, Law YZ, Chong TC. Sub-30 nm lithography with near-field scanning optical microscope combined with femtosecond laser. *Appl Phys A* **80**, 461–465 (2005).
21. Li Y, Hong MH. Parallel laser micro/nano-processing for functional device fabrication. *Laser Photonics Rev* **14**, 1900062 (2020).
22. Chen L, Cao KQ, Li YL, Liu JK, Zhang SA et al. Large-area straight, regular periodic surface structures produced on fused

silica by the interference of two femtosecond laser beams through cylindrical lens. *Opto-Electron Adv* **4**, 200036 (2021).
23. Li LJ, Gattass RR, Gershgoren E, Hwang H, Fourkas JT. Achieving λ/20 resolution by one-color initiation and deactivation of polymerization. *Science* **324**, 910–913 (2009).
24. Li ZZ, Wang L, Fan H, Yu YH, Chen QD et al. O-FIB: far-field-induced near-field breakdown for direct nanowriting in an atmospheric environment. *Light Sci Appl* **9**, 41 (2020).
25. Lin ZY, Liu HG, Ji LF, Lin WX, Hong MH. Realization of ~10 nm features on semiconductor surfaces via femtosecond laser direct patterning in far field and in ambient air. *Nano Lett* **20**, 4947–4952 (2020).
26. Li ZQ, Allegre O, Li L. Realising high aspect ratio 10 nm feature size in laser materials processing in air at 800 nm wavelength in the far-field by creating a high purity longitudinal light field at focus. *Light Sci Appl* **11**, 339 (2022).
27. Wu GX, Zhou Y, Hong MH. Sub-50 nm optical imaging in ambient air with 10× objective lens enabled by hyper-hemi-microsphere. *Light Sci Appl* **12**, 49 (2023).
28. Lin ZY, Ji LF, Li L, Liu J, Wu Y et al. Laser microsphere lens array fabrication of micro/nanostructures with tunable enhanced SERS behavior in dipole superposition Plasmon mode. *IEEE Photonics J* **9**, 2700511 (2017).
29. Feng D, Weng D, Wang B, Wang JD. Laser pulse number dependent nanostructure evolution by illuminating self-assembled microsphere array. *J Appl Phys* **122**, 243102 (2017).
30. Lim CS, Hong MH, Lin Y, Chen GX, Senthil Kumar A et al. Submicron surface patterning by laser irradiation through microlens arrays. *J Mater Process Technol* **192–193**, 328–333 (2007).
31. Jacassi A, Tantussi F, Dipalo M, Biagini C, Maccaferri N et al. Scanning probe photonic nanojet lithography. *ACS Appl Mater Interfaces* **9**, 32386–32393 (2017).
32. Yan B, Yue LY, Norman Monks J, Yang XB, Xiong DX et al. Superlensing plano-convex-microsphere (PCM) lens for direct laser nano-marking and beyond. *Opt Lett* **45**, 1168–1171 (2020).
33. Luo H, Yu HB, Wen YD, Zheng JC, Wang XD et al. Direct writing of silicon oxide nanopatterns using photonic nanojets. *Photonics* **8**, 152 (2021).
34. Chimmalgi A, Choi TY, Grigoropoulos CP, Komvopoulos K. Femtosecond laser aperturless near-field nanomachining of metals assisted by scanning probe microscopy. *Appl Phys Lett* **82**, 1146–1148 (2003).
35. Chen LW, Zhou Y, Li Y, Hong MH. Microsphere enhanced optical imaging and patterning: from physics to applications. *Appl Phys Rev* **6**, 021304 (2019).
36. Zhou Y, Hong MH, Fuh JYH, Lu L, Lukyanchuk BS et al. Near-field enhanced femtosecond laser nano-drilling of glass substrate. *J Alloys Compd* **449**, 246–249 (2008).
37. Dong WL, Liu HL, Behera JK, Lu L, Ng RJH et al. Wide bandgap phase change material tuned visible photonics. *Adv Funct Mater* **29**, 1806181 (2019).
38. Lu L, Dong ZG, Tijiptoharsono F, Ng RJH, Wang HT et al. Reversible tuning of Mie resonances in the visible spectrum. *ACS Nano* **15**, 19722–19732 (2021).
39. Choi C, Mun SE, Sung J, Choi K, Lee SY et al. Hybrid state engineering of phase-change metasurface for all-optical cryptography. *Adv Funct Mater* **31**, 2007210 (2021).
40. Iwase H, Kokubo S, Juodkazis S, Misawa H. Suppression of ripples on ablated Ni surface via a polarization grating. *Opt Express* **17**, 4388–4396 (2009).
41. Mizeikis V, Kowalska E, Juodkazis S. Resonant localization, enhancement, and polarization of optical fields in nano-scale interface regions for photo-catalytic applications. *J Nanosci Nanotechnol* **11**, 2814–2822 (2011).
42. Kaiser W, Garrett CGB. Two-photon excitation in CaF_2: Eu^{2+}. *Phys Rev Lett* **7**, 229–231 (1961).
43. Malinauskas M, Farsari M, Piskarskas A, Juodkazis S. Ultrafast laser nanostructuring of photopolymers: a decade of advances. *Phys Rep* **533**, 1–31 (2013).
44. Denk W, Strickler JH, Webb WW. Two-photon laser scanning fluorescence microscopy. *Science* **248**, 73–76 (1990).
45. Kawata S, Sun HB, Tanaka T, Takada K. Finer features for functional microdevices. *Nature* **412**, 697–698 (2001).
46. Sugioka K, Cheng Y. Femtosecond laser three-dimensional micro- and nanofabrication. *Appl Phys Rev* **1**, 041303 (2014).
47. Joglekar AP, Liu HH, Meyhöfer E, Mourou G, Hunt AJ. Optics at critical intensity: applications to nanomorphing. *Proc Natl Acad Sci USA* **101**, 5856–5861 (2004).
48. Jin F, Liu J, Zhao YY, Dong XZ, Zheng ML et al. λ/30 inorganic features achieved by multi-photon 3D lithography. *Nat Commun* **13**, 1357 (2022).
49. Roberts DE, du Plessis A, Botha LR. Femtosecond laser ablation of silver foil with single and double pulses. *Appl Surf Sci* **256**, 1784–1792 (2010).
50. Liu CP, Wang HE, Ng TW, Chen ZH, Zhang WF et al. Hybrid photovoltaic cells based on ZnO/Sb_2S_3/P_3HT heterojunctions. *Phys Status Solidi B* **249**, 627–633 (2012).
51. Zhou Y, Hong MH. Formation of a three-dimensional bottle beam via an engineered microsphere. *Photonics Res* **9**, 1598–1606 (2021).
52. Zhou Y, Ji R, Teng JH, Hong MH. Wavelength-tunable focusing via a Fresnel zone microsphere. *Opt Lett* **45**, 852–855 (2020).

Acknowledgements

This work is supported by Academic Research Fund Tier 2, Ministry of Education - Singapore (MOE2019-T2-2-147). T.C. acknowledges support from the National Key Research and Development Program of China (2019YFA0709100, 2020YFA0714504).

Author contributions

Prof. M. H. Hong and Prof. T. Cao contributed to the original experimental design. Dr. Z. Y. Lin and Mr. K. Liu contributed to the main experiments. All the authors contributed to the manuscript writing and revision.

Competing interests

The authors declare no competing financial interests.

Supplementary information

Supplementary information for this paper is available at https://doi.org/10.29026/oea.2023.230029